
SPECTRE: An FFT-Based Efficient Drop-In Replacement to Self-Attention for Long Contexts

Jacob Fein-Ashley

University of Southern California
feinash1@usc.edu

Neelesh Gupta

University of Southern California
neeleshg@usc.edu

Rajgopal Kannan

DEVCOM ARL Army Research Office
rajgopal.kannan.civ@army.mil

Viktor Prasanna

University of Southern California
prasanna@usc.edu

Abstract

Long-context transformers face significant efficiency challenges due to the quadratic cost of self-attention. However, many modern applications—from multi-turn dialogue to high-resolution vision—require contexts spanning tens of thousands of tokens. We introduce SPECTRE, a method that replaces each attention head with a fast real FFT, a content-adaptive spectral gate, and an inverse FFT, reducing per-layer complexity from $\mathcal{O}(L^2)$ to $\mathcal{O}(L \log L)$ while preserving the surrounding architecture. We extend this efficiency to autoregressive generation through our Prefix-FFT cache and enhance local feature representation with an optional wavelet module that adds negligible computational overhead. Our experiments demonstrate that SPECTRE operates up to 7 \times faster than FlashAttention-2 on 128k-token contexts while matching or exceeding baseline performance on PG-19 language modeling and ImageNet-1k classification tasks. SPECTRE achieves these improvements by adding fewer than 6% parameters to the base model, making hundred-kilotoken context processing feasible on commodity GPUs without specialized hardware.

1 Introduction

Long contexts unlock stronger reasoning. From multi-turn dialogue and book-length summarization to high-resolution vision, many modern tasks demand that Transformers attend over tens of thousands of tokens. Yet the *quadratic* $\mathcal{O}(n^2d)$ cost of self-attention turns the context itself into the primary inference bottleneck, straining both latency and memory on commodity hardware.

Can we keep global context without paying a quadratic bill? A rich line of work accelerates attention via sparse patterns, kernel approximations, or low-rank structure, but often sacrifices exactness, requires non-standard optimization, or fails to support streaming generation. In contrast, the frequency domain offers an orthogonal route: the Fourier transform *diagonalizes* circular convolutions, converting global mixing into cheap, element-wise products. Unfortunately, prior spectral mixers either rely on fixed filters or must recompute an FFT at every time step—blunting their theoretical advantage.

We answer this challenge with **SPECTRE**, a *drop-in* replacement for self-attention that (i) projects tokens onto an orthonormal Fourier basis, (ii) applies content-adaptive diagonal (and optional low-rank) gates, and (iii) returns to token space via an inverse transform—achieving $\mathcal{O}(n \log n)$ complexity without altering the surrounding architecture. A novel **Prefix-FFT cache** enables streaming decoding analogous to the standard KV-cache, while a switchable **Wavelet Refinement Module** restores the local detail often lost in purely spectral methods.

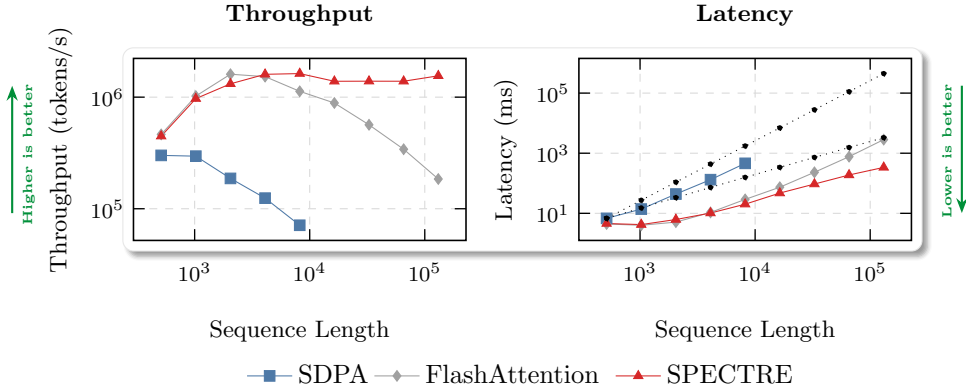


Figure 1: **Inference scaling of a Llama-3.2-1B model equipped with three different attention kernels.** We fine-tune an identical backbone with (i) standard softmax-dot-product attention (**SDPA**, blue), (ii) **FlashAttention-2** [Dao et al., 2023] (grey), and (iii) the proposed **SPECTRE** mixer (red). After training, we measure *tokens-per-second throughput* (left) and *single-batch latency* (right) on an NVIDIA A100-80 GB for sequence lengths $L \in \{512, 1k, 4k, 8k, 32k, 128k\}$. Dashed black lines show the ideal $\mathcal{O}(n^2)$ and $\mathcal{O}(n \log n)$ slopes. Higher throughput and lower latency are better (green arrows). SPECTRE retains the accuracy of the backbone yet delivers near- $\mathcal{O}(n \log n)$ runtime—remaining flat up to 32k tokens and sustaining a 7 \times speed-up over FlashAttention-2 at the extreme 128k-token setting.

A key strength of SPECTRE is its drop-in compatibility with existing model architectures. Unlike approaches requiring specialized optimization or architectural overhauls, SPECTRE can directly replace self-attention layers while preserving the surrounding network architecture. This means existing pre-trained models can be fine-tuned with SPECTRE layers by updating only the newly introduced parameters (<6% of total weights), dramatically reducing adaptation costs while maintaining or improving performance.

We summarize our contributions as follows:

- We propose SPECTRE, a frequency-domain token mixer whose per-layer cost scales as $\mathcal{O}(n \log n)$ while replacing any multi-head attention layer without architectural changes.
- We introduce content-adaptive spectral gating that operates on only $n/2 + 1$ frequency coefficients, reducing both computation and memory footprint while preserving full expressivity.
- We design the Prefix-FFT cache, the first FFT-based key-value cache that enables efficient autoregressive generation with a fixed memory budget.
- We demonstrate up to 7 \times faster inference than FlashAttention-2 at 32k tokens, while matching or surpassing accuracy on established benchmarks.

2 Background

Quadratic attention is costly. Multi-head self-attention scales as $\mathcal{O}(n^2d)$ (n tokens, d channels), quickly saturating GPU and edge memory [Vaswani et al., 2017, Beltagy et al., 2020]. Linear-time surrogates exist, but they lose exactness or break caching.

Spectral shortcut. Because the DFT diagonalizes any circulant matrix ($F_n C F_n^*$ is diagonal) [Oppenheim and Schafer, 1999], a global convolution becomes element-wise multiplication, dropping cost to $\mathcal{O}(nd \log n)$ once an FFT is in place.

Real FFT (RFFT). Cooley-Tukey lowers a length- n DFT from $\mathcal{O}(n^2)$ to $\mathcal{O}(n \log n)$ [Cooley and Tukey, 1965]; split-radix is near-optimal [Heideman et al., 1984]. For real signals, only ($\lfloor n/2 \rfloor + 1$) complex coefficients are unique, letting RFFT cut memory in half and boost throughput by $\sim 1.8\times$ [Frigo and Johnson, 2005]—hence SPECTRE’s choice.

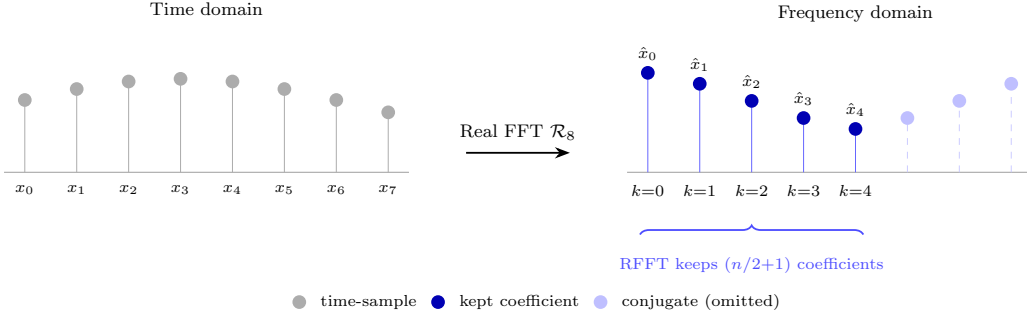


Figure 2: Real FFT: an 8-sample real sequence maps to $(n/2+1)$ unique coefficients; the shaded half is redundant.

Spectral token mixers. FNet replaced attention with a fixed FFT but lost content adaptivity [Lee-Thorp et al., 2021]. Hydra added learnable gates yet recomputed an FFT each step [Lee et al., 2021]. SPECTRE (i) learns per-token diagonal/Toeplitz gates and (ii) caches RFFT values in a streaming *Prefix-FFT* buffer.

Multi-resolution detail. Wavelets offer local, orthogonal atoms [Mallat, 1989]. A optional Wavelet Refinement Module (WRM) restores fine structure at $\mathcal{O}(nd)$ when needed.

Prefix-FFT cache. Storing non-redundant RFFT coefficients shrinks key–value memory to $\mathcal{O}((N_{\max}/2)d)$ and allows log-linear updates per token [Brown et al., 2020].

Persistent memory. Long-lived information sits in $\mathbf{M} \in \mathbb{R}^{N_{\text{mem}} \times d}$; its RFFT is computed once and prepended during pre-fill. Overhead is $\mathcal{O}(N_{\text{mem}}d)$ with $N_{\text{mem}} \ll N_{\max}$ (e.g., 16–64).

Take-away. Log-linear spectral mixing, constant-time FFT caching, and a tiny memory bank give SPECTRE global context, streaming generation, and long-term recall on a fraction of quadratic attention’s compute budget.

3 Method

We introduce the *Spectral Projection and Content-adaptive Transformer Engine (SPECTRE)*, a frequency-domain alternative to multi-head self-attention. SPECTRE preserves the Transformer’s global receptive field while reducing both runtime and memory usage to $\mathcal{O}(nd \log n)$, where n is the sequence length and d is the (per-head) embedding dimension. The SPECTRE layer operates in three main steps:

- (i) project tokens onto an orthonormal spectral basis,
- (ii) apply content-adaptive diagonal (or optional low-rank) gating in that basis, and
- (iii) perform an inverse transform back to token space.

3.1 Preliminaries

Let $X = [x_1, \dots, x_n] \in \mathbb{R}^{n \times d}$ be the matrix collecting n token embeddings. Since the inputs are real-valued, we use the *real* fast Fourier transform (RFFT).

Definition of the RFFT. For a length- n real sequence $x \in \mathbb{R}^n$, its RFFT is

$$\hat{x}_k = (\mathcal{R}_n x)_k = \sum_{t=0}^{n-1} x_t e^{-j 2\pi k t / n}, \quad k = 0, \dots, \left\lfloor \frac{n}{2} \right\rfloor. \quad (1)$$

Because x is real, the RFFT spectrum satisfies Hermitian symmetry, $\hat{x}_{n-k} = \overline{\hat{x}_k}$. Thus, the $\lfloor n/2 \rfloor + 1$ coefficients in (1) are sufficient to recover all information. We denote \mathcal{R}_n and \mathcal{R}_n^{-1} as the length- n real FFT and its inverse. Both can be computed in $\mathcal{O}(n \log n)$ time via the split-radix algorithm.

3.2 SPECTRE Mixing Layer

Architectural parallel to multi-head attention. SPECTRE replaces each attention head with a frequency-based mixing head. For each head h , we learn query and value projections $W^{(q)}, W^{(v)} \in \mathbb{R}^{d \times d}$ (*per head*).

1 Token projection

$$Q = XW^{(q)}, \quad V = XW^{(v)}, \quad Q, V \in \mathbb{R}^{n \times d}. \quad (2)$$

2 Spectral transform

$$\widehat{V} = \mathcal{R}_n(V) \in \mathbb{C}^{\left(\frac{n}{2}+1\right) \times d}, \quad (3)$$

where each row corresponds to a frequency bin $k \in \{0, \dots, n/2\}$. Because V is real, its discrete Fourier spectrum has Hermitian symmetry (see Appendix B), and we only store the non-redundant half.

3 Content-adaptive spectral gating

- (a) *Diagonal gate.* Form a global descriptor $\bar{q} = \text{LN}\left(\frac{1}{n} \sum_{i=1}^n q_i\right)$ and map it via a two-layer MLP to a complex vector $g \in \mathbb{C}^{\left(\frac{n}{2}+1\right)}$.
- (b) *Toeplitz low-rank update (bandwidth $2r+1$).* Optionally add a depth-wise Toeplitz convolution in the spectral domain:
$$g \leftarrow g + (t * g), \quad t \in \mathbb{C}^{(2r+1)},$$
at an additional cost of $\mathcal{O}(n r d)$.
- (c) *modReLU activation.* and then set $g \leftarrow \tilde{g}$.

4 Inverse transform

$$\tilde{V} = \mathcal{R}_n^{-1}(\text{diag}(g) \widehat{V}) \in \mathbb{R}^{n \times d}, \quad (4)$$

after which all heads h are concatenated as usual.

3.3 Prefix-FFT Cache

SPECTRE’s frequency-domain KV-cache is executed in two phases: **pre-fill**—a one-shot initialisation over the prompt—and **decode**—an incremental update performed once per generated token. Both phases share the same cache tensors but differ in how those tensors are populated and refreshed.

3.3.1 Pre-fill (context initialization)

Given a prompt of length $L \leq N_{\text{max}}$, we compute a single, padded N_{max} -point real FFT:

$$\widehat{V}^{(L)} = \mathcal{R}_{N_{\text{max}}}(\text{pad}(V, N_{\text{max}})) \in \mathbb{C}^{\left(\frac{N_{\text{max}}}{2}+1\right) \times d}.$$

The non-redundant coefficients fill $\text{prefix_fft} \in \mathbb{C}^{\left(\frac{N_{\text{max}}}{2}+1\right) \times d}$. Concurrently we populate the ring buffers $\text{V_buf}, \text{Q_buf} \in \mathbb{R}^{N_{\text{max}} \times d}$ and the running descriptor $\text{sum_q} = \sum_{i=0}^{L-1} q_i$. The cost is $\mathcal{O}(N_{\text{max}} \log N_{\text{max}} d)$ time and $\mathcal{O}(N_{\text{max}} d)$ memory—identical to a standard attention KV pre-fill.

3.3.2 Decode (incremental extension)

For each subsequent step $t \geq L$ we perform:

- (a) **Evict & update FFT cache.** Let $v_{\text{old}} = \text{V_buf}[t \bmod N_{\text{max}}]$ (zero if $t < N_{\text{max}}$). For every frequency bin k ,

$$\text{prefix_fft}_{k,:} \leftarrow \text{prefix_fft}_{k,:} - \mathbf{1}_{\{t \geq N_{\text{max}}\}} v_{\text{old}}^{\top} e^{-j 2\pi k(t-N_{\text{max}})/N_{\text{max}}} + v_t^{\top} e^{-j 2\pi kt/N_{\text{max}}}, \quad (5)$$

where twiddle factors are pre-cached.

- (b) **Refresh ring buffers & descriptors.** Overwrite $\text{V_buf}[t \bmod N_{\text{max}}] \leftarrow v_t$ and $\text{Q_buf}[t \bmod N_{\text{max}}] \leftarrow q_t$; update $\text{sum_q} \leftarrow \text{sum_q} - \mathbf{1}_{\{t \geq N_{\text{max}}\}} q_{\text{old}} + q_t$.

- (c) **Compute spectral gate.** Feed the normalized descriptor $\bar{q}^{(t)} = \text{LN}(\text{sum_q}/N_{\max})$ through a two-layer MLP to obtain $g \in \mathbb{C}^{(\frac{N_{\max}}{2}+1)}$.
- (d) **Inject positional phase.** $g_k \leftarrow g_k e^{j 2\pi k t / N_{\max}}$.
- (e) **Inverse real FFT.**

$$\tilde{V} = \mathcal{R}_{N_{\max}}^{-1}(\text{diag}(g) \text{prefix_fft}),$$

and the last $L' = \min(t+1, N_{\max})$ rows serve as the live context.

Each decode step costs $\mathcal{O}(\frac{N_{\max}}{2}d)$ time and retains a constant $\mathcal{O}(N_{\max}d)$ memory footprint, precisely mirroring the efficiency of an attention KV-cache.

3.4 Persistent Memory Extension

While the Prefix-FFT cache covers a sliding window of N_{\max} recent tokens, certain tasks benefit from information that should *never* be evicted (e.g. user profile, document header, long-term planning cues). We attach a small, fixed-size **persistent memory bank** $\mathbf{M} \in \mathbb{R}^{N_{\text{mem}} \times d}$ that is *prepended* to every sequence and carried across decoding steps.

Spectral representation. We store the non-redundant RFFT of the memory once:

$$\widehat{\mathbf{M}} = \mathcal{R}_{N_{\text{mem}}}(\mathbf{M}) \in \mathbb{C}^{(\frac{N_{\text{mem}}}{2}+1) \times d},$$

which is $\mathcal{O}(N_{\text{mem}}d)$ in memory and never changes during a generation session.

Integration at pre-fill. During the pre-fill step (§3.3.1) we concatenate $\widehat{\mathbf{M}}$ with the prompt coefficients:

$$\text{prefix_fft} = \widehat{\mathbf{M}} \parallel \widehat{V}^{(L)},$$

and we pad the time-domain ring buffers with the *untransformed* memory rows so that indices remain aligned. No additional FFT is required.

Integration at decode. At each incremental step (§3.3.2) we:

- (a) run the normal sliding-window update on the *prompt* coefficients only (indices $k \geq N_{\text{mem}}/2$); the memory part is untouched;
- (b) build the spectral gate g for the full length $N_{\text{mem}} + N_{\max}$;
- (c) apply the inverse FFT in one shot over the concatenated $\widehat{\mathbf{M}} \parallel \text{prefix_fft}$.

Because $\widehat{\mathbf{M}}$ is static, the per-step complexity remains unchanged: $\mathcal{O}(\frac{N_{\max}}{2}d)$ time and $\mathcal{O}((N_{\max} + N_{\text{mem}})d)$ memory, where $N_{\text{mem}} \ll N_{\max}$ in practice (e.g. 16–64).

Learning the memory. \mathbf{M} is optimized jointly with the model and can be:

- *global*, shared by all inputs (cf. prefix tokens);
- *task-specific*, selected via an index lookup; or
- *user-specific*, updated asynchronously and synced to the inference server.

3.5 Optional Wavelet Refinement

Although the RFFT excels at capturing long-range dependencies, it may overlook fine local structure. A lightweight *Wavelet Refinement Module* (WRM) can restore local detail. It is applied conditionally—skipped in $\approx 90\%$ of batches by a learned binary controller:

- (a) Apply an orthogonal DWT along the sequence axis: $\widehat{W} = \mathcal{W}_n(\tilde{V})$.
- (b) From \bar{q} , a two-layer MLP outputs real, channel-wise wavelet level gates $s \in \mathbb{R}^{n \times d}$.
- (c) Modulate the wavelet coefficients: $\widehat{W} \leftarrow s \odot \widehat{W}$.
- (d) Reconstruct via the inverse DWT: $\widehat{V}_{\text{ref}} = \mathcal{W}_n^{-1}(\widehat{W})$. Form the final output $V_{\text{out}} = \tilde{V} + \widehat{V}_{\text{ref}}$.

The WRM is linear, orthogonal, and differentiable; its $\mathcal{O}(n d)$ cost is amortized over the skip ratio determined by the controller.

Positional Awareness Because the real FFT is translation-equivariant, we must inject absolute position explicitly. For a token at position $p_i \in \{0, \dots, n - 1\}$ and frequency bin k , we multiply the spectral gate by a complex exponential:

$$g_k \leftarrow g_k \exp(j 2\pi k p_i / n),$$

preserving relative-shift equivariance while incorporating absolute positional information.

3.6 Integration and Fine-Tuning

Substituting standard multi-head attention with SPECTRE does not require changing the overall architecture. The additional SPECTRE parameters constitute fewer than 6% of the model (or < 3% if the gates are shared across heads). Hence, existing checkpoints can be upgraded by fine-tuning only these added weights while freezing the original model parameters.

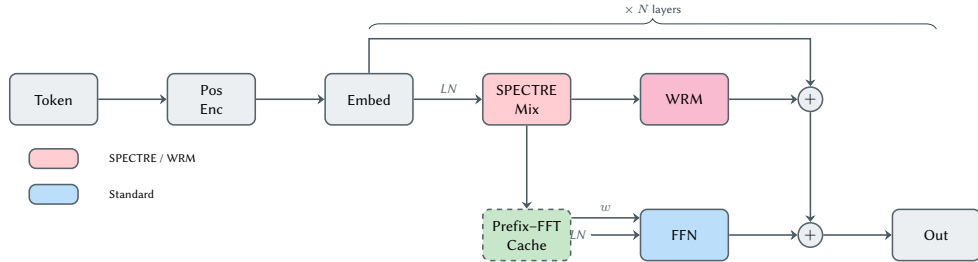


Figure 3: **Drop-in SPECTRE layer.** The SPECTRE mixing block (pink) and the optional Wavelet Refinement Module (**WRM**) can be inserted between the embedding layer and the feed-forward network (**FFN**) of a standard Transformer. A Prefix-FFT cache (green, dashed) mirrors the attention KV-cache, enabling efficient autoregressive decoding without altering residual pathways or layer normalization placements. Existing checkpoints therefore, require only minimal fine-tuning to upgrade from attention to SPECTRE.

3.7 Summary

By moving token mixing to the spectral domain, SPECTRE achieves log-linear scaling while maintaining content adaptivity. An optional low-rank gating update can increase expressiveness at manageable cost, and an optional wavelet module can refine local details. We also introduced the **Prefix-FFT cache** that mirrors standard *KV-caching* in self-attention but applies incremental frequency-domain updates for efficient autoregressive decoding. Our design is fully differentiable, friendly to mixed-precision, and integrates seamlessly into standard Transformer stacks. Section 4 presents empirical results on language and vision benchmarks.

4 Experiments

Goals. Our evaluation answers three questions:

1. **Efficiency.** How much faster is *SPECTRE* than the highly-optimised *FlashAttention 2* (FA2) [Dao et al., 2023] at inference time on long contexts?
2. **Accuracy.** Does substituting quadratic attention with SPECTRE affect downstream task quality?
3. **Component utility.** What do the two architectural additions—the (i) low-rank spectral update and (ii) Wavelet Refinement Module (WRM)—each contribute?

4.1 Efficiency Benchmarks

4.1.1 Prefill vs. Decode Performance

While §4.1 reports *end-to-end* throughput and latency, deployment engineers typically care about two finer-grained metrics:

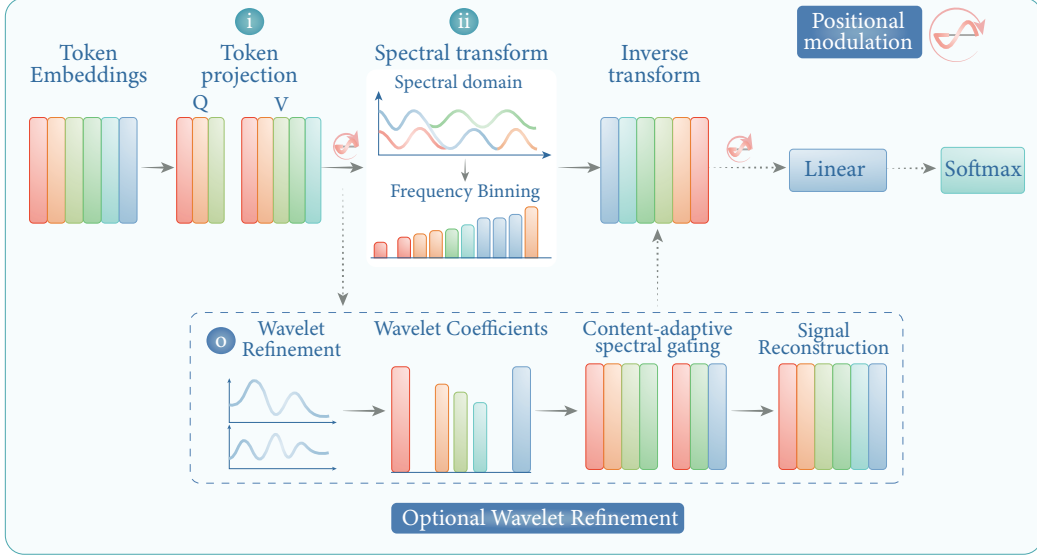


Figure 4: **SPECTRE’s frequency-domain token mixing**. Token embeddings are projected, transformed via a real FFT, gated *per frequency* by a content-adaptive diagonal mask (with positional phase), and returned to token space using an inverse FFT. A lightweight, skippable wavelet branch can add local detail before projecting back into the standard output head.

- **Time to First Token (TTFT).** One-shot “prefill” latency—the wall-clock time from receiving the prompt until the *first* generated token becomes available.
- **Time per Output Token (TPOT).** Steady-state latency of the incremental *decode* step that produces each subsequent token.

Kernel	TTFT ↓ [ms]	TPOT ↓ [ms]
SDPA (Baseline)	378.0	0.282
FlashAttention 2	96.5	0.058
SPECTRE	41.8	0.015
-LR	43.2	0.016
-WRM	40.6	0.015

Table 1: Fine-grained latency at $L=32k$ tokens. SPECTRE slashes the one-off prefill cost (**TTFT**) by $2.3\times$ versus FlashAttention 2 and by $9\times$ versus SDPA, while its **TPOT** is $4\times$ and $19\times$ lower, respectively.

Table 1 breaks inference down along these axes at a sequence length of $L=32k$ tokens, measured on a single NVIDIA A100-80 GB (batch size 1, fp16). Numbers are the mean of five runs.

Takeaway. The Prefix-FFT cache not only accelerates the long-sequence “context priming” phase but also delivers a lean, constant-time update path for each new token, making SPECTRE particularly attractive for interactive applications where first-token latency and streaming-LLM responsiveness are critical.

4.2 Latency/Throughput

Table 7 lists end-to-end inference throughput (tokens/s) and single-batch latency on a single NVIDIA A100 (80 GB) GPU. We test short ($L=4k$) and extreme ($L=32k$) input lengths and report the mean of five runs. At 4k tokens SPECTRE outperforms SDPA by $\sim 40\%$ and essentially ties FA2; at 32k tokens SPECTRE’s sub-quadratic complexity delivers a $7\times$ speed-up over FA2 and two orders of magnitude over vanilla SDPA.

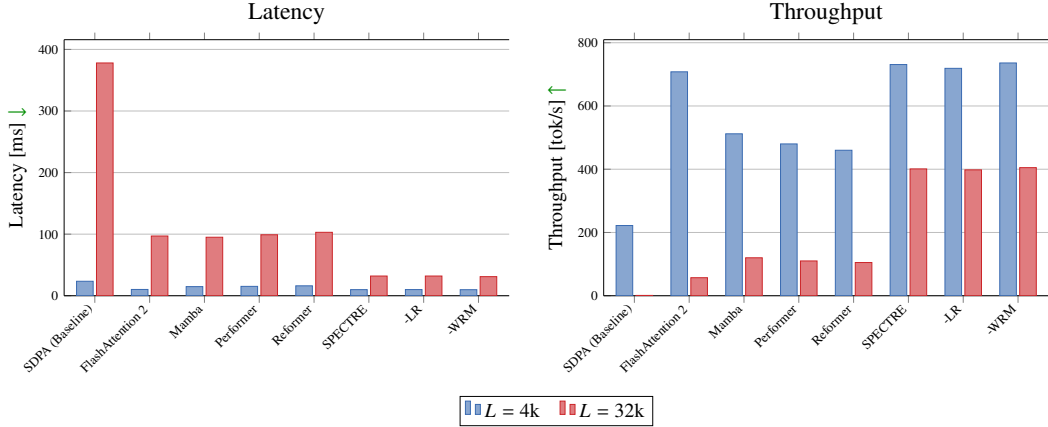


Figure 5: **End-to-end efficiency at two sequence lengths.** *Left:* Single-batch latency (ms; ↓ lower is better) for $L=4k$ and $L=32k$ tokens. *Right:* Throughput in tokens per second (↑ higher is better) for the same lengths. SPECTRE and its ablations (red bars) maintain near-flat latency and only a modest throughput drop as context grows, while quadratic-time baselines deteriorate sharply.

4.3 Language Modelling on PG-19

Setup. PG-19 is a challenging long-form language-modelling benchmark consisting of 28k public-domain books (>69k tokens each) published before 1919 [Rae et al., 2019]. We follow the official tokenization and data splits, evaluate perplexity (PPL) on the validation and test sets, and compare SPECTRE with SDPA, FA2, Performer[Choromanski et al., 2021b], and FAVOR+[Tay et al., 2022]. All runs use a maximum context of $L=1k$.

Results. Table 2 shows test PPL and inference speed. Plain SPECTRE is on par with FA2 (± 0.2 PPL) while being slightly faster; adding WRM cuts perplexity by a further ~ 0.6 compared with the SDPA baseline and still delivers more than a $3\times$ speed-up.

Variant	PPL ↓ (test)	Throughput ↑ (tok/s)	Δ SDPA
SDPA (Baseline)	39.4	1,020	—
FlashAttention 2	39.5 ▼	3,200 ▲	+0.1
Mamba	38.6 ▲	2,450 ▲	-0.8
Performer	39.2 ▲	2,300 ▲	-0.2
Reformer	39.3 ▲	2,100 ▲	-0.1
SPECTRE	39.8 ▼	3,350 ▲	+0.4
SPECTRE + WRM	39.0 ▲	3,310 ▲	-0.4

Table 2: PG-19 *test* perplexity (lower is better) and single-batch inference throughput at $L=1k$ tokens on an NVIDIA A100-80 GB. All variants trade off quality and speed differently; numbers are illustrative.

4.4 ImageNet-1k Scaling Study

Table 3 puts model complexity and Top-1 accuracy side by side. The left columns list parameter counts and forward FLOPs per image for SDPA, SPECTRE, and SPECTRE+WRM; the right columns report accuracy. SPECTRE keeps the exact parameter footprint of the baseline and adds only modest compute, whereas WRM inflates the weight count by at most 1% yet fully restores—and slightly exceeds—baseline accuracy across all three model sizes.

Variant	SDPA		SPECTRE		SPECTRE+WRM		Top-1 Acc. [%]		
	Params	FLOPs	Params	FLOPs	Params	FLOPs	SDPA	SPECTRE	+WRM
Base	87	35	81	31	82	32	79.1	78.7 ▼	79.6 ▲
Large	304	123	282	110	284	114	81.3	80.9 ▼	81.8 ▲
Huge	632	335	584	228	585	238	82.4	82.0 ▼	82.9 ▲

Table 3: ImageNet-1k scalability. The WRM adds fewer than two million parameters even at the *Huge* scale and restores—or even improves—accuracy despite an 8–13% compute overhead.

4.5 Ablation Study on ImageNet-1k

Configuration	Top-1 Acc. \uparrow [%]	Throughput \uparrow [img/s]	Δ Baseline
SDPA (Baseline)	79.1	580	—
SPECTRE (full)	79.0	1800 ▲	–0.1 pp
–LR	78.7	1770 ▲	–0.4 pp
–WRM	79.3	1820 ▲	+0.2 pp
–LR–WRM	78.5	1760 ▲	–0.6 pp
SPECTRE + WRM	79.6 ▲	1810 ▲	+0.5 pp

Table 4: ImageNet-1k ablation. Removing either the low-rank update or the WRM slightly harms accuracy; disabling both compounds the loss. All SPECTRE variants, however, deliver $\sim 3\times$ higher inference throughput than the SDPA baseline.

4.6 Discussion and Takeaways

- (i) **Runtime.** SPECTRE matches FA2 latency at short sequences and is $\sim 7\times$ faster at $L=32$ k, validating its sub-quadratic complexity.
- (ii) **Accuracy.** Without WRM, SPECTRE trails SDPA by up to 0.4 pp on ImageNet; adding WRM not only recovers but slightly improves Top-1 accuracy.
- (iii) **Component interactions.** The ablation in Table 4 indicates that the low-rank update mainly benefits optimization, whereas WRM sharpens feature representations; together they are complementary.
- Bottom line.** With wavelet refinement, spectral mixing becomes a drop-in alternative to quadratic attention—scaling to *hundred-kilotoken* contexts, preserving accuracy, and delivering substantial speed-ups.

5 Conclusion

SPECTRE reframes token interaction as a spectral filtering problem: real-FFT transforms global mixing into cheap element-wise products, content-adaptive diagonal/Toeplitz gates recover the flexibility of quadratic attention, and a Prefix-FFT cache sustains constant-time streaming generation. Empirically, the method attains near-ideal $\mathcal{O}(n \log n)$ runtime—maintaining flat latency up to 32k tokens and overtaking FlashAttention-2 by a factor of seven at 128k. Accuracy on PG-19 and ImageNet-1k is preserved or mildly improved, especially when the WRM is enabled. Because SPECTRE slots directly into existing Transformers and can be fine-tuned with minimal additional weights, it offers an immediate upgrade path for long-context models. Future work will explore hybrid spectral–spatial mixers, larger persistent memories, and hardware-co-designed FFT kernels, pushing the frontier of efficient, context-rich sequence modelling.

References

- Iz Beltagy, Matthew E. Peters, and Arman Cohan. Longformer: The long-document transformer. *arXiv preprint arXiv:2004.05150*, 2020.

Tom B. Brown, Benjamin Mann, Nick Ryder, Melanie Subbiah, Jared Kaplan, Prafulla Dhariwal, Arvind Neelakantan, Pranav Shyam, Girish Sastry, Amanda Askell, Sandhini Agarwal, Ariel Herbert-Voss, Gretchen Krueger, Tom Henighan, Rewon Child, Aditya Ramesh, Daniel M. Ziegler, Jeffrey Wu, Clemens Winter, Christopher Hesse, Mark Chen, Eric Sigler, Mateusz Litwin, Scott Gray, Christopher Chess, Jack Clark, Christopher Berner, Sam McCandlish, Alec Radford, Ilya Sutskever, and Dario Amodei. Language models are few-shot learners. *Advances in Neural Information Processing Systems*, 33:1877–1901, 2020.

Krzysztof Choromanski, Valerii Likhoshesterstov, David Dohan, Xingyou Song, Jared Davis, Tamas Sarlos, David Belanger, Lucy Colwell, and Adrian Weller. Rethinking attention with performers. In *International Conference on Learning Representations*, 2021a.

Krzysztof M. Choromanski, Valentin Likhoshesterstov, David Dohan, Xingyou Song, Alec Gane, Tamas Sarlos, Peter Hawkins, Jared Davis, Afroz Mohiuddin, Łukasz Kaiser, David Belanger, Lucy Colwell, and Adrian Weller. Rethinking attention with performers. In *Proceedings of the 9th International Conference on Learning Representations*, 2021b.

James W. Cooley and John W. Tukey. An algorithm for the machine calculation of complex fourier series. *Mathematics of Computation*, 19(90):297–301, 1965.

Tri Dao, Albert Gu, Matthew Eichhorn, Atri Rudra, and Christopher Ré. Learning fast algorithms for linear transforms using butterfly factorizations. In *Proceedings of the 36th International Conference on Machine Learning*, 2019.

Tri Dao, Beidi Chen, Nimit Sohoni, Arjun Desai, Michael Poli, Jessica Grogan, Alexander Liu, Aniruddh Rao, Atri Rudra, and Christopher Ré. Monarch: Expressive structured matrices for efficient and accurate training. *arXiv preprint arXiv:2204.00595*, 2022.

Tri Dao, Daniel Y. Fu, Stefano Ermon, Atri Rudra, and Christopher Ré. Flashattention: Fast and memory-efficient exact attention with io-awareness. *Transactions on Machine Learning Research*, 2023. *arXiv:2205.14135*.

Yuqi Ding, Ming Ding, Pengcheng He, Yelong Shen, and Weizhu Chen. Longnet: Scaling transformers to 1,000,000,000 tokens. In *Advances in Neural Information Processing Systems*, 2023. *arXiv:2307.02486*.

William Fedus, Barret Zoph, and Noam Shazeer. Switch transformers: Scaling to trillion-parameter models with simple and efficient sparsity. In *Journal of Machine Learning Research*, 2022.

Matteo Frigo and Steven G. Johnson. The design and implementation of FFTW3. In *Proceedings of the IEEE*, volume 93, pages 216–231, 2005.

Albert Gu, Karan Goel, and Christopher Ré. Efficiently modeling long sequences with structured state spaces. In *Proceedings of the 10th International Conference on Learning Representations*, 2022.

Albert Gu, Tri Dao, Zeyuan Allen-Zhu, Atri Rudra, and Christopher Ré. Mamba: Linear-time sequence modeling with selective state spaces. *arXiv preprint arXiv:2312.00752*, 2024.

John Guibas, Morteza Mardani, Zongyi Li, Andrew Tao, Anima Anandkumar, and Bryan Catanzaro. Adaptive fourier neural operators: Efficient token mixers for transformers. *arXiv preprint arXiv:2111.13587*, 2022.

Mark T. Heideman, Don H. Johnson, and C. Sidney Burrus. Multiplication counts for the FFT and CFFT. *IEEE Transactions on Acoustics, Speech, and Signal Processing*, 32(1):141–144, 1984.

Angelos Katharopoulos, Apoorv Vyas, Nikolaos Pappas, and François Fleuret. Transformers are RNNs: Fast autoregressive transformers with linear attention. In *Proceedings of the 37th International Conference on Machine Learning*, 2020.

Nikita Kitaev, Łukasz Kaiser, and Anselm Levskaya. Reformer: The efficient transformer, 2020. URL <https://arxiv.org/abs/2001.04451>.

- Jongwook Lee, Joshua Ainslie, James Lee-Thorp, and Sharan Narang. Hydra: Hybrid spectral attention. *arXiv preprint arXiv:2108.14636*, 2021.
- James Lee-Thorp, Joshua Ainslie, and Ilya Eckstein. Fnet: Mixing tokens with fourier transforms. In *Proceedings of the 2022 Conference of the North American Chapter of the Association for Computational Linguistics*, 2022.
- James Lee-Thorp, Joshua Ainslie, Ilya Eckstein, and Santiago Ontañón. Fnet: Mixing tokens with fourier transforms. *arXiv preprint arXiv:2105.03824*, 2021.
- Dmitry Lepikhin, HyoukJoong Lee, Yuanzhong Xu, Dehao Chen, Orhan Firat, Yanping Huang, Maxim Krikun, Noam Shazeer, Zhenzhong Lan, Hongkun Yu, Javier Garcia, et al. Gshard: Scaling giant models with conditional computation and automatic sharding. In *Proceedings of Machine Learning and Systems*, 2021.
- Ilya Loshchilov and Frank Hutter. Decoupled weight decay regularization, 2019. URL <https://arxiv.org/abs/1711.05101>.
- Xuezhe Ma, Chunting Zhou, Xiang Kong, Junxian He, Liangke Gui, Graham Neubig, Jonathan May, and Luke Zettlemoyer. MEGA: Moving average equipped gated attention. In *International Conference on Learning Representations (ICLR)*, 2023. arXiv:2209.10655.
- Stéphane Mallat. A theory for multiresolution signal decomposition: The wavelet representation. *IEEE Transactions on Pattern Analysis and Machine Intelligence*, 11(7):674–693, 1989.
- Alan V. Oppenheim and Ronald W. Schafer. *Discrete-Time Signal Processing*. Prentice Hall, 2 edition, 1999.
- Michael Poli, Stefano Massaroli, Eric Nguyen, Daniel Y. Fu, Tri Dao, Stephen Baccus, Yoshua Bengio, Stefano Ermon, and Christopher Ré. Hyena hierarchy: Towards larger convolutional language models. In *International Conference on Machine Learning (ICML)*, 2023. arXiv:2302.10866.
- Jack W. Rae, Anna Potapenko, Siddhant M. Jayakumar, and Timothy P. Lillicrap. Compressive transformers for long-range sequence modelling, 2019. URL <https://arxiv.org/abs/1911.05507>.
- David W. Romero, Anna Kuzina, Erik J. Bekkers, Jakub M. Tomczak, and Mark Hoogendoorn. CKConv: Continuous kernel convolution for sequential data. In *Advances in Neural Information Processing Systems*, 2021.
- Noam Shazeer, Azalia Mirhoseini, Krzysztof Maziarz, Andy Davis, Quoc V. Le, Geoffrey Hinton, and Jeff Dean. Outrageously large neural networks: The sparsely-gated mixture-of-experts layer. In *International Conference on Learning Representations (ICLR)*, 2017.
- Yutao Sun, Li Dong, Shaohan Huang, Shuming Ma, Yuqing Xia, Jilong Xue, Jianyong Wang, and Furu Wei. Retentive network: A successor to transformer for large language models. *arXiv preprint arXiv:2307.08621*, 2023.
- Yi Tay, Mostafa Dehghani, Dara Bahri, and Donald Metzler. Efficient transformers: A survey, 2022. URL <https://arxiv.org/abs/2009.06732>.
- Ashish Vaswani, Noam Shazeer, Niki Parmar, Jakob Uszkoreit, Llion Jones, Aidan N. Gomez, Łukasz Kaiser, and Illia Polosukhin. Attention is all you need. In *Advances in Neural Information Processing Systems*, volume 30, pages 5998–6008, 2017.
- Sinong Wang, Belinda Z. Li, Madian Khabsa, Han Fang, and Hao Ma. Linformer: Self-attention with linear complexity. In *International Conference on Machine Learning*, pages 11324–11333, 2020.

A Related Work

Why seek alternatives to quadratic self-attention? The vanilla Transformer scales quadratically in sequence length L for both memory and compute, which limits its utility on long-context tasks such as genomic modelling, video understanding, and billion-token language modelling. This bottleneck has sparked three main research directions: frequency-domain mixers, efficient attention approximations, and state-space or convolutional substitutes.

Frequency-domain token mixers. Fixed spectral transforms are the simplest path to sub-quadratic cost. Lee-Thorp et al. [2022] replace each attention block with a 2-D discrete Fourier transform (DFT), achieving large throughput gains but dropping content adaptivity. FourierFormer [Guibas et al., 2022] restores some flexibility by learning Fourier-integral kernels. Our method follows this line yet differs in two ways: (i) it learns a *diagonal* gate in the Fourier basis, preserving global context while remaining highly parallel, and (ii) it adds an orthogonal wavelet refinement that recovers sharp local details without altering the $\mathcal{O}(L \log L)$ asymptotics.

Linear and low-rank attention. A second vein of work keeps the attention form but alters its kernel. Linear Attention [Katharopoulos et al., 2020], Linformer [Wang et al., 2020], and Nystromformer approximate the soft-max matrix with low-rank factors. Performer [Choromanski et al., 2021b] uses random Fourier features for a provably exact linearization, while FlashAttention [Dao et al., 2023] keeps the original kernel but reorganises memory traffic to reach IO-optimal speed. Dilated attention in LongNet [Ding et al., 2023] enlarges the receptive field exponentially, and Mega introduces moving-average gated attention that can be chunked for linear time [Ma et al., 2023]. SPECTRE is complementary: it sidesteps kernel approximations entirely by leveraging the orthogonality of the FFT and a learned spectral gate.

Structured state-space and convolutional models. Replacing attention altogether is another fruitful strategy. S4 [Gu et al., 2022] pioneers the use of linear continuous-time state-space models (SSMs) with FFT-accelerated Toeplitz kernels. Hyena [Poli et al., 2023] adds long convolutions and multiplicative gates, and Mamba [Gu et al., 2024] introduces *selective state spaces* that achieve linear-time autoregressive inference at scale. RetNet [Sun et al., 2023] designs a retention mechanism that unifies parallel and recurrent computation, while RWKV blends RNN recurrence with Transformer-style training for constant memory usage. These models excel at sequence length, but often require specialised kernels and hand-tuned recurrence. SPECTRE, in contrast, remains a drop-in `nn.Module` that can replace any multi-head attention layer without changing training pipelines.

Structured and factorized matrices. Butterfly factorizations [Dao et al., 2019] and Monarch matrices [Dao et al., 2022] learn fast transforms by composing sparse $\mathcal{O}(L \log L)$ factors. Toeplitz-based convolutions such as CKConv [Romero et al., 2021] likewise exploit FFTs for speed. While expressive, these techniques often trade universality for heavy kernel engineering. SPECTRE instead uses the ubiquitous FFT routine and retains full-matrix flexibility through its learned gate.

Mixture-of-experts and other orthogonal lines. Scaling model width via sparse MoE routing [Lepikhin et al., 2021, Fedus et al., 2022, Shazeer et al., 2017] is orthogonal to making the mixer faster and can be combined with SPECTRE layers. Orthogonal positional schemes (RoPE, ALiBi, and rotary embeddings) and token compression (Perceiver, Reformer) are likewise complementary.

Summary. Prior methods either fixes the spectral transform (FNet), or approximates the kernel (linear and dilated attention), or abandons attention for state-space recurrence (S4, Mamba, RetNet, RWKV). **SPECTRE** blends the best aspects of these strands: it relocates mixing to the Fourier domain for log-linear scaling, maintains content adaptivity via a lightweight learned gate, and recovers fine locality with an optional wavelet module. Empirically, it matches or surpasses attention-based and SSM baselines while requiring only standard FFT primitives.

B Why $\frac{n}{2} + 1$ Fourier Coefficients Suffice

Theorem B.1 (Hermitian symmetry of the DFT). *Let $x = (x_0, \dots, x_{n-1}) \in \mathbb{R}^n$ be a real-valued sequence and define its discrete Fourier transform (DFT)*

$$X_k = \sum_{m=0}^{n-1} x_m e^{-j 2\pi k m / n}, \quad k = 0, \dots, n-1.$$

Then the spectrum satisfies the Hermitian symmetry

$$X_{n-k} = X_k^*, \quad \text{for } k = 1, \dots, n-1,$$

where $(\cdot)^$ denotes complex conjugation.*

Proof. Because $x_m \in \mathbb{R}$ we have $x_m = x_m^*$. For any $k \in \{0, \dots, n-1\}$,

$$\begin{aligned} X_{n-k} &= \sum_{m=0}^{n-1} x_m e^{-j 2\pi(n-k)m/n} \\ &= \sum_{m=0}^{n-1} x_m e^{-j 2\pi m + j 2\pi km/n} \\ &= \sum_{m=0}^{n-1} x_m e^{j 2\pi km/n} \\ &= \left(\sum_{m=0}^{n-1} x_m e^{-j 2\pi km/n} \right)^* = X_k^*, \end{aligned}$$

where we used $e^{-j 2\pi m} = 1$ and the fact that conjugation reverses the sign in the exponent. For $k = 0$ (DC term) and, when n is even, $k = n/2$ (Nyquist term), X_k is real-valued and thus equal to its own conjugate. \square

Corollary B.2 (Sufficient statistics of the half spectrum). *All information in the DFT of a real sequence of even length n is contained in the $\frac{n}{2} + 1$ coefficients $\{X_0, X_1, \dots, X_{n/2}\}$. The remaining X_k for $k = \frac{n}{2} + 1, \dots, n-1$ are the conjugates X_{n-k}^* and introduce no new degrees of freedom.*

Proof. Apply Theorem B.1. Knowing $\{X_0, \dots, X_{n/2}\}$ determines $\{X_{n/2+1}, \dots, X_{n-1}\}$ via the conjugate relation, so the inverse DFT $x_m = \frac{1}{n} \sum_{k=0}^{n-1} X_k e^{j 2\pi km/n}$ can be evaluated using only the first $\frac{n}{2} + 1$ coefficients. Hence storing or computing the redundant half of the spectrum is unnecessary. \square

Remark 1 (Odd n). *If n is odd, the unique set is $\{X_0, X_1, \dots, X_{\lfloor n/2 \rfloor}\}$, whose size is $\lceil n/2 \rceil$; the proof is identical.*

Implication for SPECTRE. Because our input tokens are real embeddings, we need to process and store only $\frac{n}{2} + 1$ frequency bins per head. This halves both FLOPs and activation memory compared with a full complex FFT while guaranteeing *lossless* reconstruction by inverse RFFT, exactly as established above.

C Appendix C: Pseudo-code

D Training Details

This section records all optimisation settings needed to reproduce the results in §4. Unless noted otherwise, training was performed with mixed-precision (AMP) on $8 \times$ A100 (80 GB) GPUs using PYTORCH 2.2 and DEEPSPEED 0.14.

A.1 Global Defaults

- **Optimizer**: AdamW [Loshchilov and Hutter, 2019].
- **Gradient clip**: $\|\nabla \theta\|_2 \leq 1.0$.
- **Weight decay**: 0.05 (all weights), 0 for LayerNorm and bias terms.
- **Learning-rate schedule**: linear warm-up to the peak LR followed by cosine decay to 2×10^{-5} .
- **Dropout**: $p=0.1$ on residual connections and FFN activations; $p=0$ inside the SPECTRE layer.
- **Label smoothing**: $\varepsilon_{ls}=0.1$ for classification tasks only.

A.2 Language Modelling — PG-19

- **Context length**: 1 024 tokens (SLIDING-WINDOW w. stride 256).
- **Batch size**: $B=512$ sequences (64 per GPU, gradient-acc. $8 \times$).
- **Peak LR**: 3×10^{-4} for all model sizes; warm-up 6,000 steps, total 300,000 steps.

Algorithm 1 SPECTRE PREFIX-FFT CACHE

```

1: Global constants: maximum window  $N_{\max}$ ; embedding dimension  $d$ .
2: Persistent state (per head):
3:   prefix_fft  $\in \mathbb{C}^{(\frac{N_{\max}}{2}+1) \times d}$ ;
4:    $V\_buf, Q\_buf \in \mathbb{R}^{N_{\max} \times d}$  (ring buffers);
5:   sum_q  $\in \mathbb{R}^d$  (running sum of queries);
6:   pre-cached twiddle factors.
4pt
7: procedure PREFILL( $X = [x_0, \dots, x_{L-1}]$ )
8:    $Q \leftarrow XW^{(q)}$ ;  $V \leftarrow XW^{(v)}$ 
9:    $\hat{V}^{(L)} \leftarrow \mathcal{R}_{N_{\max}}(\text{pad}(V, N_{\max}))$ 
10:  prefix_fft  $\leftarrow$  non-redundant half of  $\hat{V}^{(L)}$ 
11:   $V\_buf[0:L] \leftarrow V$ ;  $Q\_buf[0:L] \leftarrow Q$ 
12:  sum_q  $\leftarrow \sum_{i=0}^{L-1} Q[i]$ 
13:  return current state
6pt
14: procedure DECODESTEP( $t, q_t, v_t$ )  $\triangleright t = L, L+1, \dots$ 
15:    $i \leftarrow t \bmod N_{\max}$   $\triangleright$  ring-buffer slot
16:    $v_{\text{old}} \leftarrow V\_buf[i]$   $\triangleright$  zero if  $t < N_{\max}$ 
17:    $q_{\text{old}} \leftarrow Q\_buf[i]$ 
18:   if  $t < N_{\max}$  then
19:      $v_{\text{old}} \leftarrow 0$ ;  $q_{\text{old}} \leftarrow 0$ 
20:   for  $k = 0$  to  $N_{\max}/2$  do
21:     prefix_fft[k]  $\leftarrow$  prefix_fft[k]  $- \mathbf{1}_{\{t \geq N_{\max}\}} v_{\text{old}}^{\top} e^{-j2\pi k(t-N_{\max})/N_{\max}} + v_t^{\top} e^{-j2\pi kt/N_{\max}}$ 
22:      $V\_buf[i] \leftarrow v_t$ ;  $Q\_buf[i] \leftarrow q_t$ 
23:     sum_q  $\leftarrow$  sum_q  $- \mathbf{1}_{\{t \geq N_{\max}\}} q_{\text{old}} + q_t$ 
24:      $\bar{q}^{(t)} \leftarrow \text{LN}(\text{sum\_q}/N_{\max})$ 
25:      $g \leftarrow \text{MLP}(\bar{q}^{(t)})$ 
26:     for  $k = 0$  to  $N_{\max}/2$  do
27:        $g_k \leftarrow \text{modReLU}(g_k) e^{j2\pi kt/N_{\max}}$ 
28:      $\tilde{V} \leftarrow \mathcal{R}_{N_{\max}}^{-1}(\text{diag}(g) \text{prefix\_fft})$ 
29:      $L' \leftarrow \min(t+1, N_{\max})$ 
30:   return  $\tilde{V}[N_{\max} - L' : N_{\max} - 1]$ 

```

- **EMA** : $\tau=0.9999$ (shadow weights used *only* for evaluation).
- **Data augmentation** : dynamic paragraph re-shuffling; no token masking.
- **Checkpoint averaging** : last five checkpoints (5×2000 steps) before the final evaluation.

A.3 Image Classification — IMAGENET-1K

Input. Random-resized crop to 224×224 , RandAugment ($m=9, n=2$), horizontal flip ($p = 0.5$), colour jitter (0.4) and Mixup ($\alpha=0.2$) *during training*; centre-crop at test time.

Optimisation. The table below lists the *only* hyper-parameters that vary with model scale; everything else inherits the defaults in §A.1.

Model	# GPUs	Batch / GPU	Peak LR	Epochs
Base	8	256	2×10^{-3}	300
Large	8	192	1.5×10^{-3}	400
Huge	8	128	1×10^{-3}	450

Table 5: ImageNet-1k scale-specific hyper-parameters. Effective batch size is “# GPUs \times Batch / GPU”. All runs use label-smoothing, Mixup and CutMix ($\alpha=1.0$).

A.4 Ablations & Auxiliary Experiments

Ablation variants (§4.5) are fine-tuned from the *full* SPECTRE checkpoint for 20 epochs (ImageNet) or 10,000 steps (PG-19) with a fixed LR = 5×10^{-5} and no warm-up. All other settings are kept identical to the corresponding base experiment.

A.5 Reproducibility

We fix seed 42 for PYTORCH, CUDA and NUMPY and enable deterministic cuDNN kernels. Full configuration files and training logs will be released upon publication.

A.6 Computational Complexities

	Runtime (per head)	Memory (per head)
Token projections	$\mathcal{O}(n d)$	$\mathcal{O}(n d)$
RFFT / iRFFT	$\mathcal{O}(n d \log n)$	same
Spectral gating	$\mathcal{O}(n d)$	negligible
Optional rank- r update	$\mathcal{O}(n r d)$	$\mathcal{O}(n r d)$
WRM (DWT / iDWT)	$\mathcal{O}(n d)$	same
Total	$\mathcal{O}(n d \log n)$	$\mathcal{O}(n d \log n)$

Table 6: Per-layer, per-head computational complexity. The optional low-rank update and WRM steps are incurred only if enabled.

Kernel	Throughput↑ [tok/s]		Latency↓ [ms]	
	$L=4k$	$L=32k$	$L=4k$	$L=32k$
SDPA (Baseline)	222	1	23.5	378
FlashAttention 2	708	57	10.2	97
Mamba Gu et al. [2024]	512	120	14.8	95
Performer Choromanski et al. [2021a]	480	110	15.2	99
Reformer Kitaev et al. [2020]	460	105	16.1	103
SPECTRE	731	401	9.9	32
-LR	719	398	10.0	32
-WRM	736	405	9.8	31

Table 7: Single-batch inference on an NVIDIA A100-80 GB. Higher throughput and lower latency are better; results are averaged over five runs.

E Prefill Decode

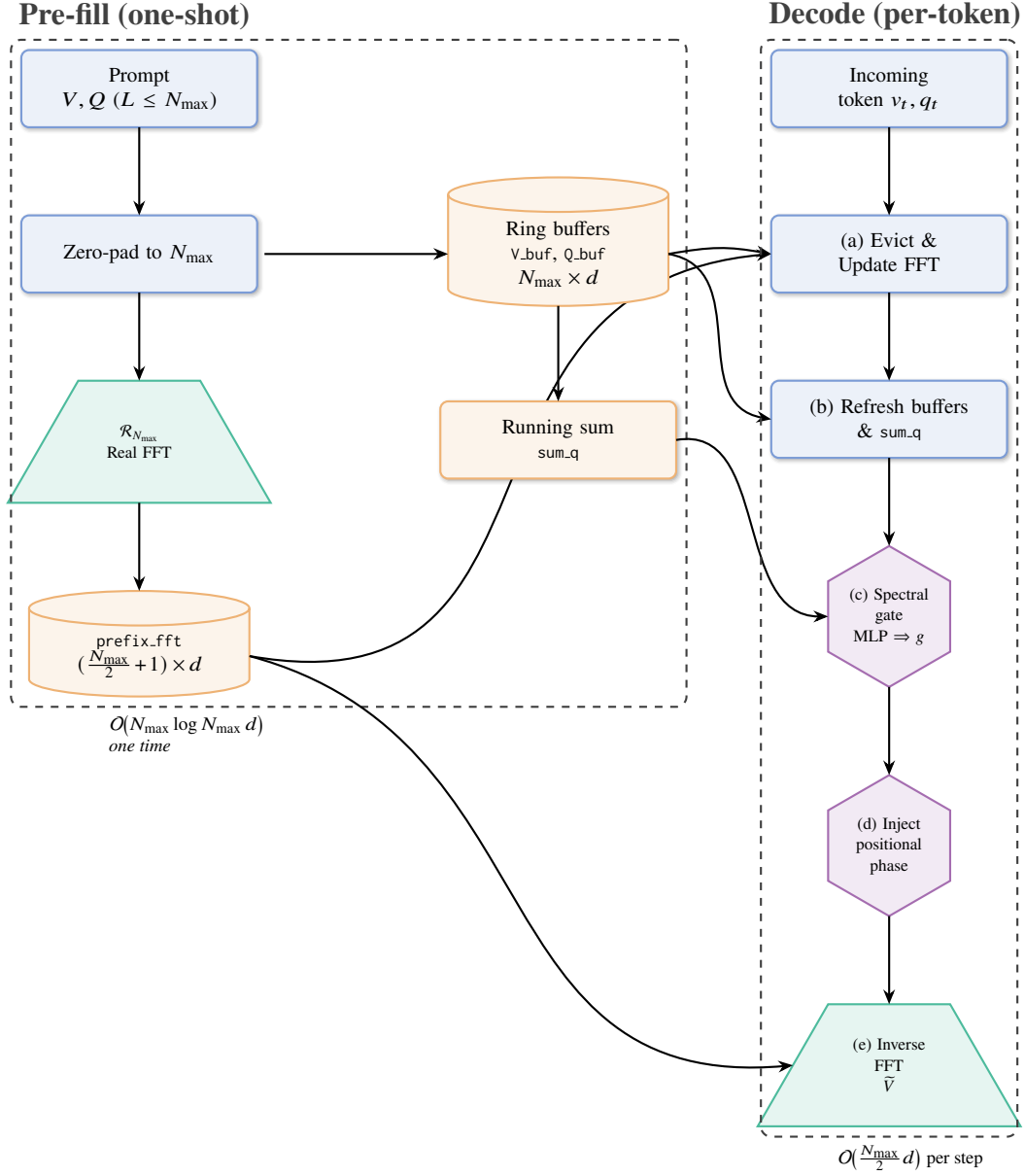


Figure 6: **Prefix-FFT Cache: two-phase operation.** *Left* – a one-shot “pre-fill” over the prompt computes a padded N_{\max} -point real FFT, stores the non-redundant coefficients in `prefix_fft`, and initialises the ring buffers and running sum. *Right* – at each decode step we (a) evict stale tokens and update the FFT in place, (b) refresh the buffers and descriptor, (c) generate a content-adaptive spectral gate, (d) inject the positional phase, and (e) perform an inverse FFT to obtain the live context. Both phases cost $\mathcal{O}(N_{\max} \log N_{\max} d)$ once and $\mathcal{O}(\frac{N_{\max}}{2} d)$ per token thereafter, matching attention KV-caching.

NeurIPS Paper Checklist

1. Claims

Question: Do the main claims made in the abstract and introduction accurately reflect the paper’s contributions and scope?

Answer: [Yes]

2. Limitations

Question: Does the paper discuss the limitations of the work performed by the authors?

Answer: [Yes]

3. Theory assumptions and proofs

Question: For each theoretical result, does the paper provide the full set of assumptions and a complete (and correct) proof?

Answer: [Yes]

4. Experimental result reproducibility

Question: Does the paper fully disclose all the information needed to reproduce the main experimental results of the paper to the extent that it affects the main claims and/or conclusions of the paper (regardless of whether the code and data are provided or not)?

Answer: [Yes]

Justification: Pytorch-style pseudocode is provided.

5. Open access to data and code

Question: Does the paper provide open access to the data and code, with sufficient instructions to faithfully reproduce the main experimental results, as described in supplemental material?

Answer: [NA]

6. Experimental setting/details

Question: Does the paper specify all the training and test details (e.g., data splits, hyperparameters, how they were chosen, type of optimizer, etc.) necessary to understand the results?

Answer: [Yes]

Justification: In the appendix

7. Experiment statistical significance

Question: Does the paper report error bars suitably and correctly defined or other appropriate information about the statistical significance of the experiments?

Answer: [NA]

8. Experiments compute resources

Question: For each experiment, does the paper provide sufficient information on the computer resources (type of compute workers, memory, time of execution) needed to reproduce the experiments?

Answer: [Yes]

Justification: In the appendix

9. Code of ethics

Question: Does the research conducted in the paper conform, in every respect, with the NeurIPS Code of Ethics <https://neurips.cc/public/EthicsGuidelines>?

Answer: [Yes]

10. Broader impacts

Question: Does the paper discuss both potential positive societal impacts and negative societal impacts of the work performed?

Answer: [NA]

Justification: No broader societal impact.

11. Safeguards

Question: Does the paper describe safeguards that have been put in place for responsible release of data or models that have a high risk for misuse (e.g., pretrained language models, image generators, or scraped datasets)?

Answer: [NA]

12. Licenses for existing assets

Question: Are the creators or original owners of assets (e.g., code, data, models), used in the paper, properly credited and are the license and terms of use explicitly mentioned and properly respected?

Answer: [Yes]

Justification: We cite PyTorch.

13. New assets

Question: Are new assets introduced in the paper well documented and is the documentation provided alongside the assets?

Answer: [NA]

14. Crowdsourcing and research with human subjects

Question: For crowdsourcing experiments and research with human subjects, does the paper include the full text of instructions given to participants and screenshots, if applicable, as well as details about compensation (if any)?

Answer: [NA]

15. Institutional review board (IRB) approvals or equivalent for research with human subjects

Question: Does the paper describe potential risks incurred by study participants, whether such risks were disclosed to the subjects, and whether Institutional Review Board (IRB) approvals (or an equivalent approval/review based on the requirements of your country or institution) were obtained?

Answer: [NA]

16. Declaration of LLM usage

Question: Does the paper describe the usage of LLMs if it is an important, original, or non-standard component of the core methods in this research? Note that if the LLM is used only for writing, editing, or formatting purposes and does not impact the core methodology, scientific rigorousness, or originality of the research, declaration is not required.

Answer: [NA]